ACS OMEGA

Open Access

http://pubs.acs.org/journal/acsodf

Article

Mass Spectrometry-Imaging Analysis of Active Ingredients in the Leaves of *Taxus cuspidata*

Xiaori Zhan, Yue Zang, Ruoyun Ma, Wanting Lin, Xiao-lin Li, Yanyan Pei, Chenjia Shen,* and Yan Jiang*

Cite This: *ACS Omega* 2024, 9, 18634−18642

Read Online

ACCESS | Metrics & More | Article Recommendations | Supporting Information

ABSTRACT: Background: *Taxus cuspidata* is an endangered evergreen conifer mainly found in Northeast Asia. In addition to the well-known taxanes, several active ingredients were detected in the leaves of *T. cuspidata*. However, the precise spatial distribution of active ingredients in the leaves of *T. cuspidata* is largely unknown. Results: in the present study, timsTOF flex MALDI-2 analysis was used to uncover the accumulation pattern of active ingredients in *T. cuspidata* leaves. In total, 3084 ion features were obtained, of which 944 were annotated according to the mass spectrometry database. The principal component analysis separated all of the detected metabolites into four typical leaf tissues: mesophyll cells, upper epidermis, lower epidermis, and vascular bundle cells. Imaging analysis identified several leaf tissues that specifically accumulated active ingredients, providing theoretical support for studying the regulation mechanism of compound biosynthesis. Furthermore, the relative accumulation levels of each identified compound were analyzed. Two flavonoid compounds, ligustroflavone and Morin, were identified with high content through quantitative analysis of the ion intensity. Conclusions: our data provides fundamental information for the protective utilization of *T. cuspidata*.

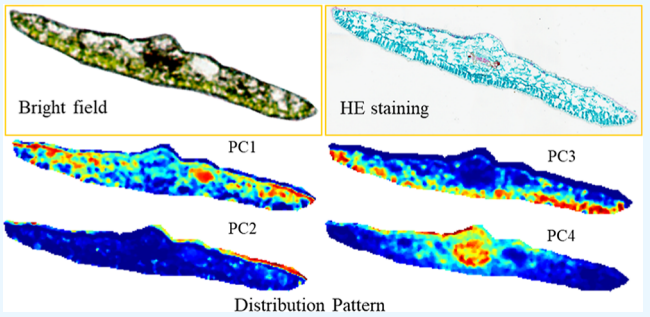

BACKGROUND

Taxus is a rare genus of dioecious, evergreen trees with significant medicinal and ecological value.[1] The *Taxus* tree is considered a valuable natural resource for taxol (also known as paclitaxel) and its derivatives, which are the most important market access anticancer drugs.[2,3] With the deterioration of the environment, the incidence of cancer is on the rise. To obtain scarce taxol, wild *Taxus* trees have suffered devastating damage.[4] The conservation and comprehensive utilization of *Taxus* trees have become a hot research focus.

Modern medical research proves that the extracts of *Taxus* twigs contain a variety of biological constituents, such as terpenoids, phenols, polysaccharides, and flavonoids.[5,6] Various compounds exhibit a wide range of pharmacological activities, making *Taxus* extracts important sources of drugs for treating different diseases.[7] From the extracts of *Taxus chinensis* fruit, 14 compounds with potential neuroprotective activity were isolated. These compounds could be used in the treatment of neuronal injury and Alzheimer's disease.[8] Ascorbic acid, carotenoids, and polyphenols extracted from *Taxus baccata* red arils exhibit strong antioxidant activities.[9] A number of flavonoids with diverse skeleton structures were reported to exhibit significant antibacterial, antiaging, and antiviral activities.[10] Using the high-performance liquid chromatography with diode-array detection method, several phenolic compounds with antioxidant and anticancer activities were determined in the *Taxus cuspidata* bark extracts.[11] α-Conidendrin, a polyphenolic compound extracted from *Taxus yunnanensis*, exhibits significant anticancer activity on human breast cancer cell lines.[12] Detailed identification of active ingredients in the *Taxus* tree contributes to the comprehensive utilization of this rare plant.

Bark contains a large number of active ingredients, but it is a nonrenewable resource. Due to its sufficient biomass and renewable characteristics, the *Taxus* leaf is a primary resource used for industrial extraction.[13] In the past few years, a number of active ingredients have been detected and isolated from the leaves of different *Taxus* species.[14] In plants, the leaf is the primary organ for photosynthesis and carbon fixation, harboring various types of tissues.[15] Previous studies have focused on the spatial distribution of medicinal components in plant leaves. In the leaf of *Arabidopsis*, lipids, such as galactolipids, accumulate highly in the interveinal leaf lamina.[16]

Received: February 14, 2024
Revised: March 27, 2024
Accepted: March 28, 2024
Published: April 10, 2024

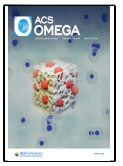

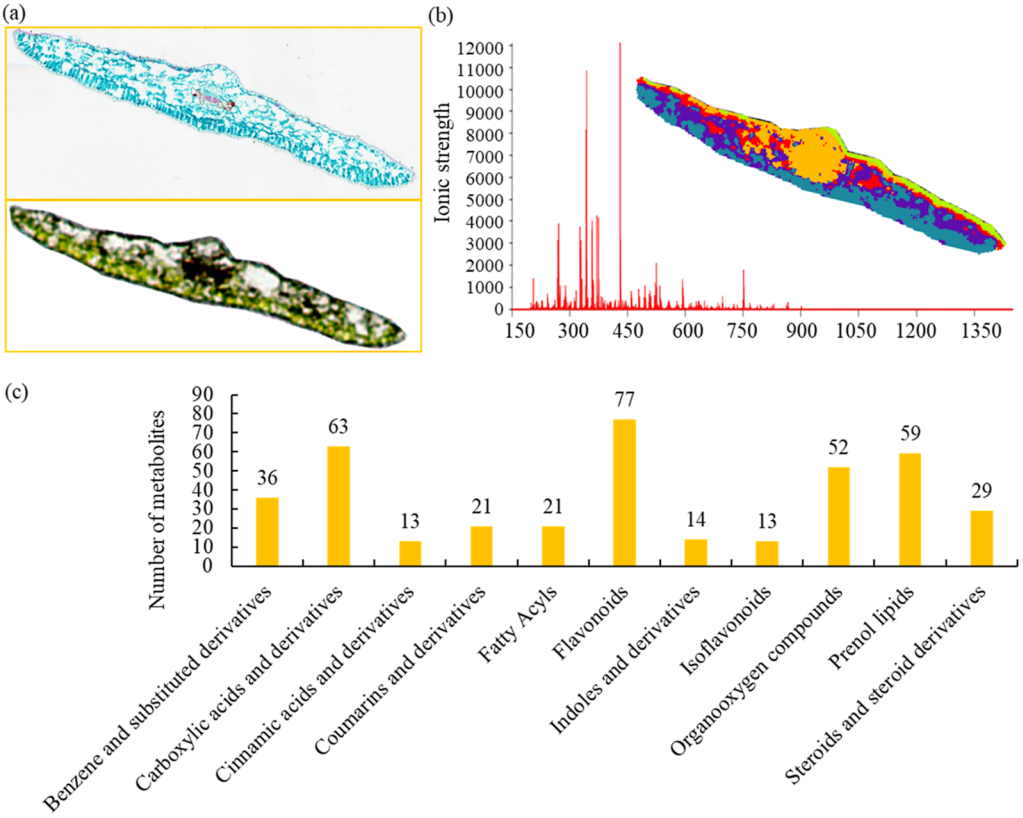

Figure 1. Analysis of the data from timsTOF fleX MALDI-2. (a) Sampling and sectioning of the *T. cuspidata* leaves. (b) Mean mass spectrogram and segmentation analysis of the *T. cuspidata* leaf sample. (c) Number of the metabolites belonging to different groups.

In *Clausena lansium*, alkaloids are especially enriched in the leaf epidermal region, while coumarins are mainly distributed in the leaf vein tissues.[17] Investigating spatial distribution patterns is crucial to understanding the biological functions of active ingredients in medicinal plants.

Mass spectrometry (MS) imaging is a newly developed in situ metabolomic technique that refers to the analysis of compounds within tissues without the need for tissue collection or extraction.[18] Traditional methods need to consider the polarity of the target compound, and MALDI-MSI is also a suitable analytical technique for both polar and nonpolar biomolecules.[19] MS imaging allows chemists to visualize the distribution of chemical molecules in a slice and determine the molecules in different locations.[20] MS imaging is a fit-for-purpose tool for detecting the transformations of secondary metabolites in plant tissues.[21] MS imaging, coupled with continuously improving MS databases, can efficiently dereplicate, identify, and quantify active ingredients in medicinal plants.[22] Principal component analysis (PCA) is a method of extracting important variables from a large set of variables available in a dataset. It extracts a low-dimensional set of features from a high-dimensional dataset with the motive to capture as much information as possible.[23] PCA can be used to divide complex features into different distribution patterns. *T. cuspidata* is an endangered evergreen conifer mainly distributed in Northeast Asia.[24]

Traditional MS technology detected a variety of bioactive metabolites in the leaves of *T. cuspidata*.[25] For example, six new taxanes with various skeletons were isolated from the needles of *T. cuspidata*.[26] Due to the tissue specificity of gene expression, understanding the location of metabolites can be helpful in deciphering their biosynthetic pathways.[13,27] Data on the spatial distribution of active ingredients can also provide guidance for sampling for the pharmaceutical industry. However, the precise spatial distribution of active ingredients in the leaves of *T. cuspidata* is largely unknown. In this study, we utilized the MALDI-IMS approach to determine the spatial distributions of different types of active compounds in the leaves of *T. cuspidata*.

RESULTS AND DISCUSSION

Overview of the TimsTOF Flex MALDI-2 Data. TimsTOF flex MALDI-2 was carried out to identify the active ingredients in the leaves of *T. cuspidata* (Figure 1a). The raw MS imaging files were imported into the SCiLS Lab workstation for MS feature identification. In total, 3084 ion features were obtained, of which 944 were annotated according to the MS database. The detailed information on each MS feature, including *m*/*z*, compound name, notation, formula, metabolite annotation, and *m*/*z*-Dev, is listed in Table S1. Segmentation analysis divided the leaf map into 7696 data points with different colors, suggesting that the data resolution meets the requirements of subsequent research (Figure 1b).

According to the annotation information, 658 ion features were grouped into various categories (Figure 1c). Among the identified metabolites, the largest number of features belonged to "flavonoids" (77 features), followed by "carboxylic acids and derivatives" (63 features), "prenol lipids" (59 features), and "organooxygen compounds" (52 features). For active ingredient-related groups, 29 steroids and derivatives, 21 coumarins and derivatives, and 13 cinnamic acids and derivatives were

https://doi.org/10.1021/acsomega.4c01440
ACS Omega 2024, 9, 18634−18642

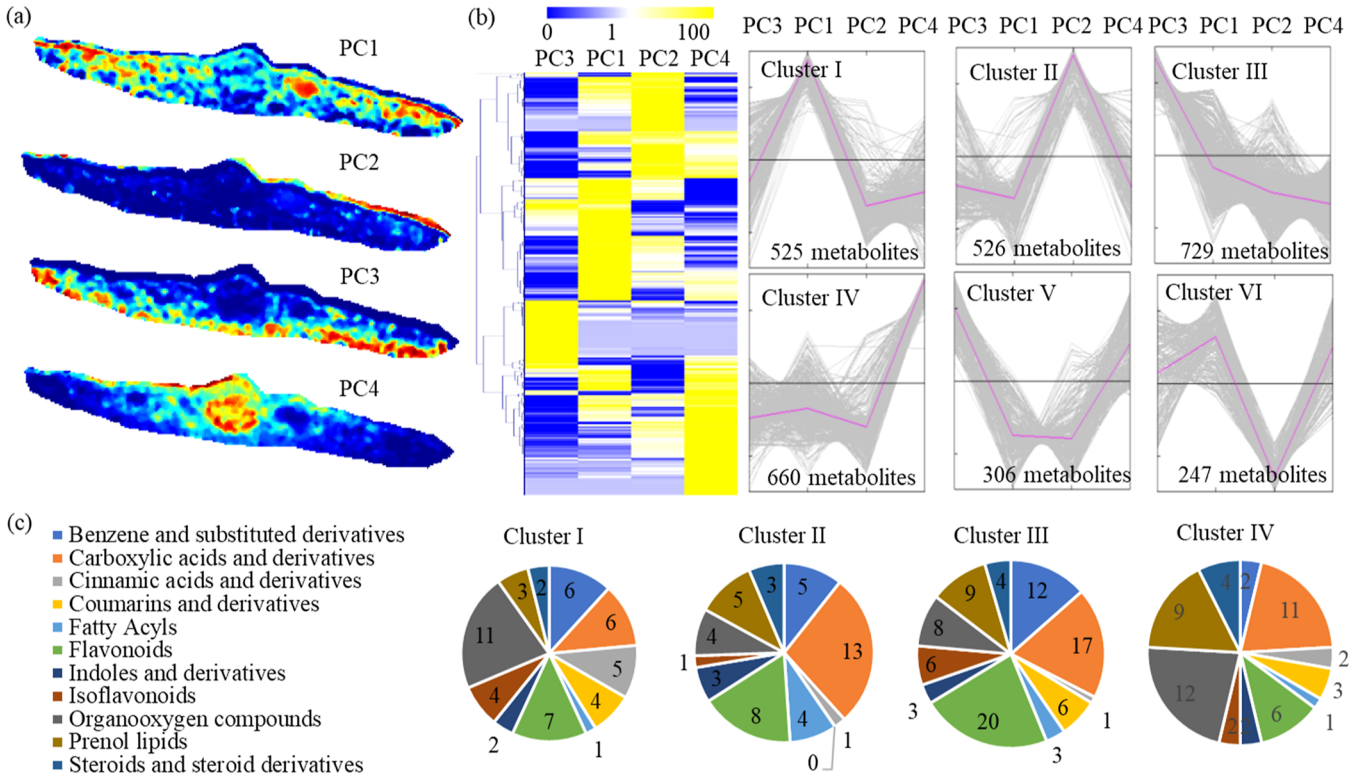

Figure 2. PCA of the identified metabolites. (a) PCA of all identified metabolites in the leaves of *T. cuspidata* leaves. PC1−PC4 indicated four different distribution patterns of identified metabolites in the *T. cuspidata* leaves. (b) Heatmap displaying the relative levels of different identified metabolites. Heatmap scale ranges from 0 to 100 on a log2 scale. Clustering analysis classed all of the identified metabolites into six clusters. (c) Number of metabolites belonging to different categories in each cluster.

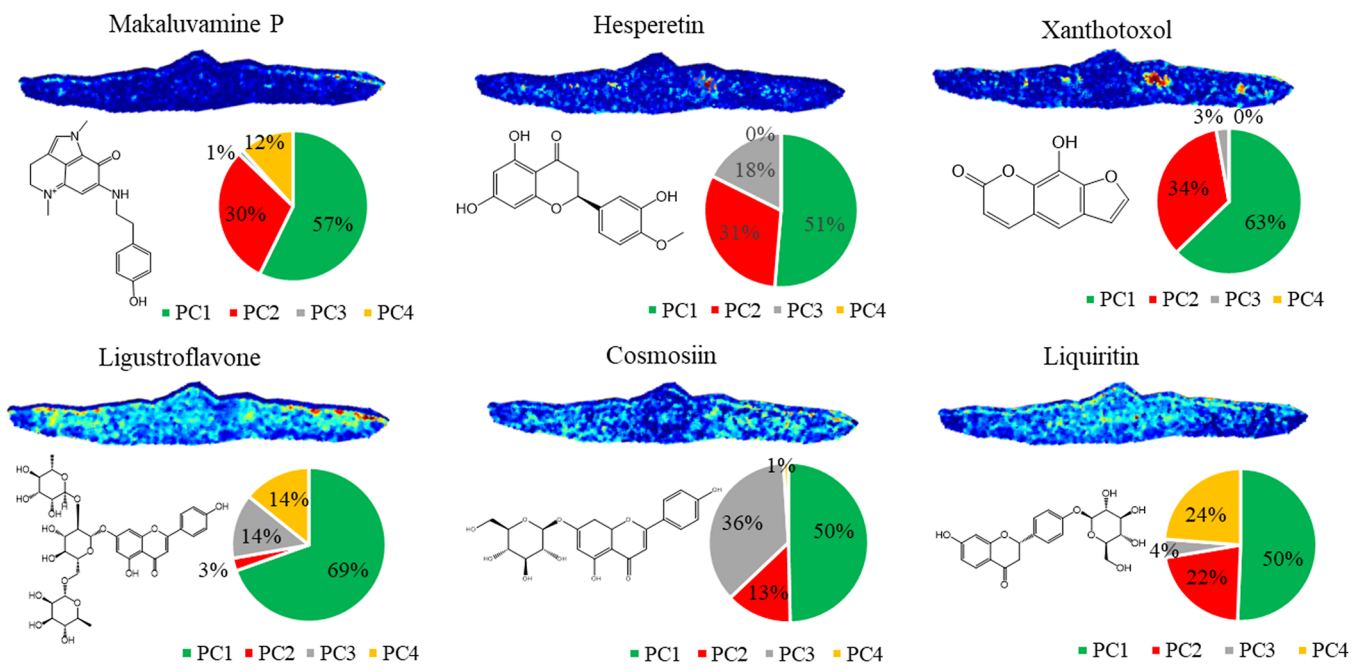

Figure 3. Imaging of mesophyll cell predominantly accumulated metabolites. Mesophyll cell predominantly accumulated metabolites were determined by MALDI-IMS analysis. Color scale ranges from 0 to 100%. Blue indicated low accumulation level and red indicated high accumulation level. Proportion of various metabolites in different PCs was showed by pies.

detected, providing reliable data for analyzing the spatial distribution of active ingredients in the leaves of *T. cuspidata*.

PCA of the Identified Metabolites. The PCA separated all the detected metabolites into four principal components (PCs), referring to typic leaf tissues: mesophyll cells (PC1), upper epidermis (PC2), lower epidermis (PC3), and epidermis/bundle sheath cells (PC4, Figure 2a). The heatmap illustrated the loading intensities of each metabolite in different

https://doi.org/10.1021/acsomega.4c01440
ACS Omega 2024, 9, 18634−18642

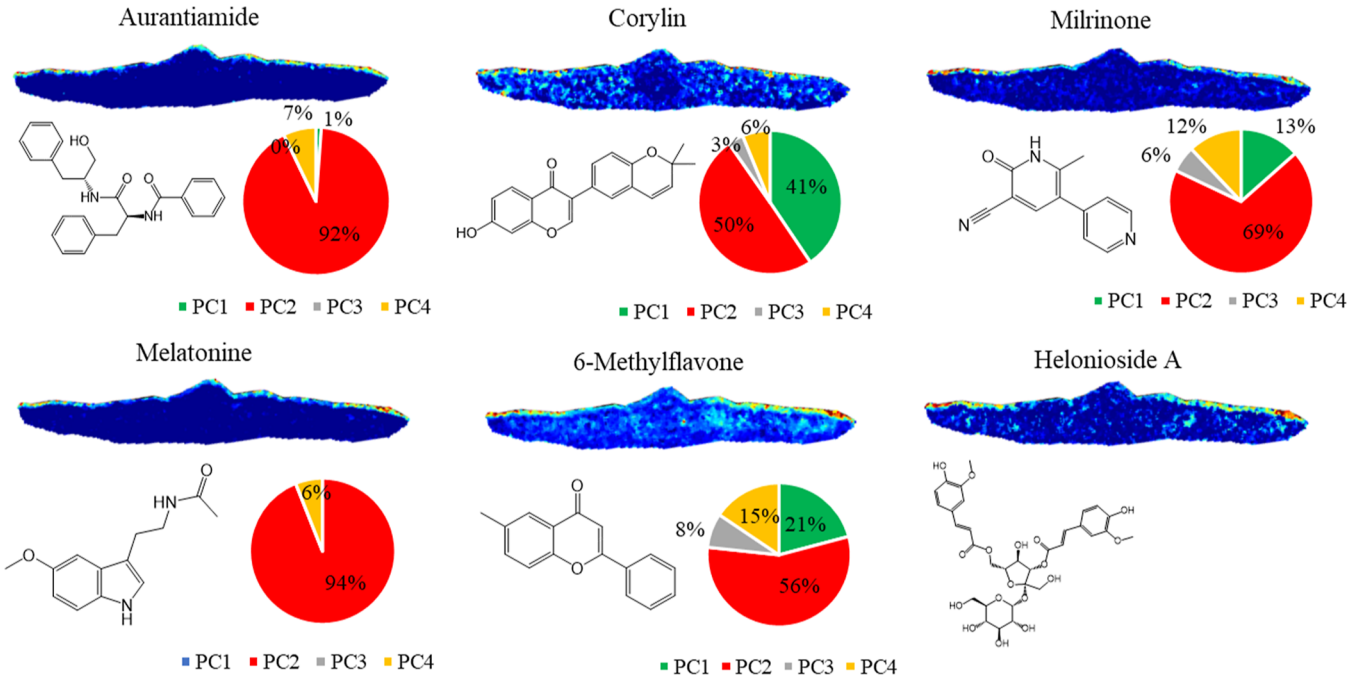

Figure 4. Imaging of upper epidermis predominantly accumulated metabolites. Upper epidermis predominantly accumulated metabolites were determined by MALDI-IMS analysis. Color scale ranges from 0 to 100%. Blue indicated low accumulation level and red indicated high accumulation level. Proportion of various metabolites in different PCs was showed by pies.

PCs (Figure 2b). Clustering analysis grouped all of the detected metabolites into six clusters. In detail, 525 metabolites were predominantly enriched in Cluster I (PC1), 526 metabolites were greatly enriched in Cluster II (PC2), 729 metabolites were significantly enriched in Cluster III (PC3), and 660 metabolites were mainly enriched in Cluster IV (PC4). In Cluster I, the "organooxygen compounds" group occupied the largest share; in Cluster II and III, the "carboxylic acids and derivatives" and "fatty acyls" groups occupied the largest shares; and in Cluster IV, "carboxylic acids and derivatives", "organooxygen compounds", and "prenol lipids" were the largest groups (Figure 2c).

ROC is a method that combines sensitivity and specificity to comprehensively evaluate discrimination effectiveness. Regions that are selected for ROC analysis were based on PCA, which can be used for ROC analysis between two regions of interest. In our study, two regions within a slice were selected for ROC analysis (Figure S1). The results of the ROC analysis are listed in Table S2.

Imaging of Mesophyll Cell Predominantly Accumulated Metabolites. A number of mesophyll cells that predominantly accumulated metabolites were identified by MALDI-IMS analysis (Figure 3). Makaluvamine P is a pyrroloiminoquinone alkaloid, known for its potent antioxidant activity.[28] Hesperetin is a flavonoid that significantly contributes to the inhibition of oxidative stress, inflammation, and apoptosis.[29] Xanthotoxol is an active coumarin that exhibits various bioactivities and pharmacological properties, such as the suppression of the inflammatory response.[30] MALDI-IMS analysis showed that makaluvamine P, hesperetin, and xanthotoxol predominantly accumulated in mesophyll cells (>50%) and secondarily accumulated in upper epidermal cells (>30%). Ligustroflavone is a flavone that was first isolated from the leaves of the common privet.[31] Our data showed that ligustroflavone significantly accumulated in the mesophyll cell (69%). Cosmosiin is a flavone glycoside that was first identified in the leaves of red *Citrus grandis*. Liquiritin is a flavonoid/phenolic derivative that has antioxidative properties.[32] In the leaves of *T. cuspidata*, ligustroflavone, cosmosiin, and liquiritin were found to be evenly distributed in the mesophyll cells.

Imaging of Upper Epidermis Predominantly Accumulated Metabolites. Six typic upper epidermal cells predominantly accumulated metabolites (>50%), such as aurantiamide, corylin, milrinone, melatonine, 6-methylflavone, and helonioside A, were identified (Figure 4). Aurantiamide and its acetylation product (aurantiamide acetate) are peptides exhibiting significant cytotoxic activity on the HL-60 leukemia human cancer cell line.[33] Melatonine is an important indole heterocyclic compound that is involved in various adaptive responses in plants.[34] Interestingly, aurantiamide and melatonine specifically accumulated in the upper epidermal cells (>90%), indicating that they are at the front line of plant defense. The active flavonoid compound, corylin, was first detected in the medicinal plant Psoralea fructus (*Psoralea corylifolia* L.).[35] In the leaves of *T. cuspidata*, potential corylin compounds were detected, which were mainly distributed in the mesophyll cells and upper epidermal cells. Moreover, helonioside A, an antioxidant phenylpropanoid glycoside, and 6-methylflavone, a flavonoid aglycone, showed a similar distribution pattern in the leaves of *T. cuspidata*.[36,37]

Imaging of Vascular Bundle Cells Predominantly Accumulated Metabolites. There are two morphologically and functionally distinct cell types: bundle sheath cells and mesophyll cells that surround the bundle sheath layer, which consists of the vascular bundles.[38] In *Papaver setiferum* leaves, the alkaloids were predominantly localized within the walls and vascular bundles of the capsules.[39] Isocolumbin is a natural alkaloids targeting the epidermal growth factor receptor in nonsmall cell lung cancer.[40] Gartanin, which is first identified in the purple mangosteen fruit, is a potent growth inhibitor of

https://doi.org/10.1021/acsomega.4c01440
ACS Omega 2024, 9, 18634−18642

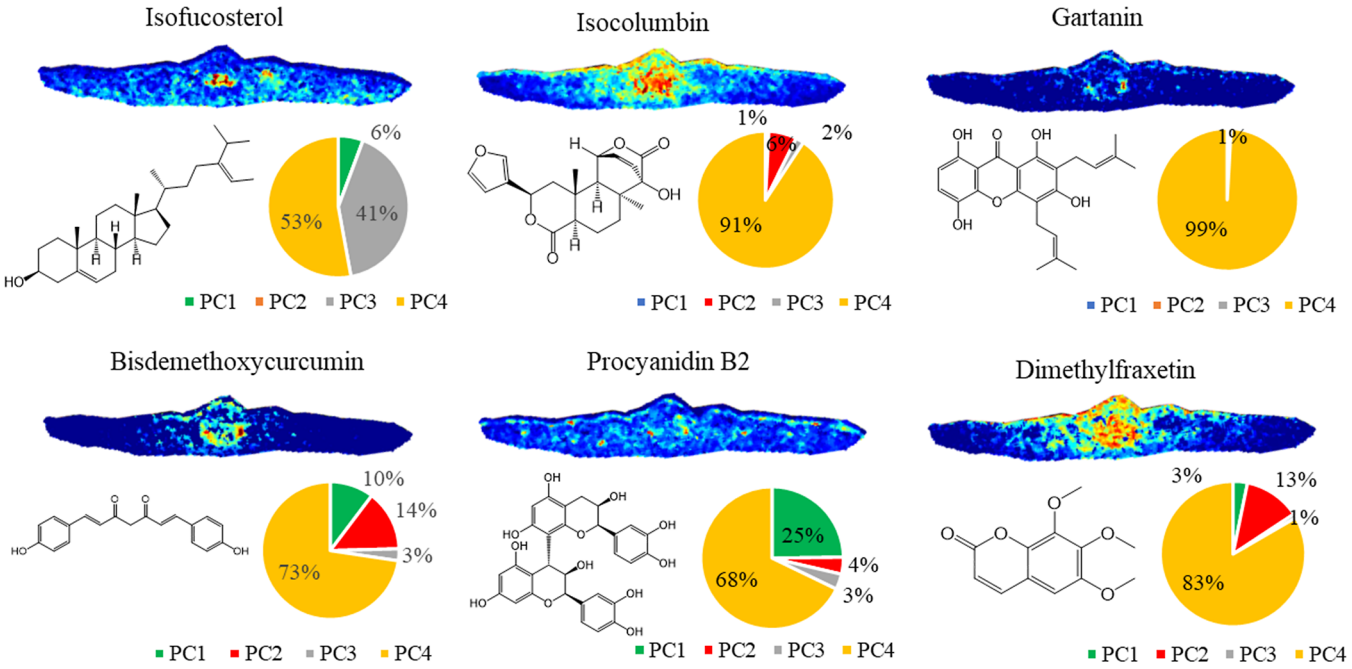

Figure 5. Imaging of epidermis/bundle sheath cells predominantly accumulated metabolites. Epidermis/bundle sheath cells predominantly accumulated metabolites were determined by MALDI-IMS analysis. Color scale ranges from 0 to 100%. Blue indicated low accumulation level and red indicated high accumulation level. Proportion of various metabolites in different PCs was showed by pies.

various cancer cell lines.[41,42] In *T. cuspidata*, isocolumbin and gartanin are two vascular bundle cell specifically accumulated active compounds (>90%), suggesting their movement between plant tissues. Procyanidin B2 is a potent natural antioxidant exhibiting multiprotective roles in response to vitrification stimuli.[43] In *T. cuspidata*, Procyanidin B2 was detected in vascular bundle cells and mesophyll cells. Additionally, bisdemethoxycurcumin and dimethylfraxetin were also significantly accumulated in the vascular system of *T. cuspidata* leaves (Figure 5).

Imaging of Metabolites Distributed Relatively Evenly. In *T. cuspidata*, a number of active compounds are evenly distributed in the leaves (Figure 6). Five active ingredients with anticancer properties, including 5,6,7-trimethoxyflavone, aromadendrin, cafestol, dihydroquercetin, and triptophenolide, were relatively evenly distributed in the leaves of *T. cuspidata*.[44−47] *T. cuspidata* contains various potential anticancer drugs, indicating its significant medicinal value. Moreover, two active ingredients (4-hydroxychalcone and Morin) with anti-inflammatory, and two active ingredients (astilbin and isopimpinellin) with antibacterial activity, were also relatively evenly distributed in the *T. cuspidata* leaves.[48−50] The leaves of *T. cuspidata* contain evenly distributed active ingredients, making them excellent raw materials for the pharmaceutical industry.

Accumulation Levels of Different Active Ingredients. The contents of different active ingredients in plant tissues vary greatly. MALDI-IMS analysis is a valuable method to reveal the relative levels of each identified compound in plant tissues.[51] Among the 27 active ingredients mentioned above, two flavonoid compounds, ligustroflavone and Morin, accumulated significantly in the leaves of *T. cuspidata* (intensity > 100). So far, a large number of flavonoids with different skeletons were isolated from *Taxus* plants. Flavonoids have potential benefits for human health and were reported to be play significant antibacterial, anti-aging, anti-Alzheimer's, antidiabetic and anticancer.[10] Our data suggest that the leaves of *T. cuspidata* are suitable raw materials for extracting ligustroflavone and Morin. Meanwhile, several active ingredients, such as makaluvamine P, xanthotoxol, aurantiamide, melatonine, isofucosterol, gartanin, procyanidin B2, 5,6,7-trimethoxyflavone, 4-hydroxychalcone, and astilbin, showed relatively low accumulation levels in the leaves of *T. cuspidata* (intensity < 10). Procyanidin B2, one of the most classic natural pigments, has numerous bioactivities and possesses the potential to prevent a wide range of human diseases.[52] The low content compounds also have very high medicinal value. In industrial extraction, artificially increasing the concentrations of these low-content compounds is a necessary step.

CONCLUSIONS

TimsTOF flex MALDI-2 was utilized to analyze the accumulation pattern of active ingredients in *T. cuspidata* leaves. The PCA separated all the detected metabolites into four typical leaf tissues: mesophyll cells, upper epidermis, lower epidermis, and vascular bundle cells. The imaging analysis identified several leaf tissue specifically accumulated active ingredients. Our data provides fundamental information for the protective utilization of *T. cuspidata*.

METHODS

Plant Samples. Three-year-old *T. cuspidata* seedlings were planted in a growth chamber at the campus of Hangzhou Normal University, Hangzhou, China. Professor Yaobin Song (Hangzhou Normal University) identified the *T. cuspidata* seedlings. A young leaf was harvested and prepared for cryosection and MS imaging analysis. All the chemicals were purchased from Sinopharm (Shanghai, China). One sample was analyzed in our study, and three replicates from the same sample were carried out.

Sampling and Sectioning. Leica CM1950 cryosection (Leica, Wetzlar, Germany) was used with a slice thickness of

https://doi.org/10.1021/acsomega.4c01440
ACS Omega 2024, 9, 18634−18642

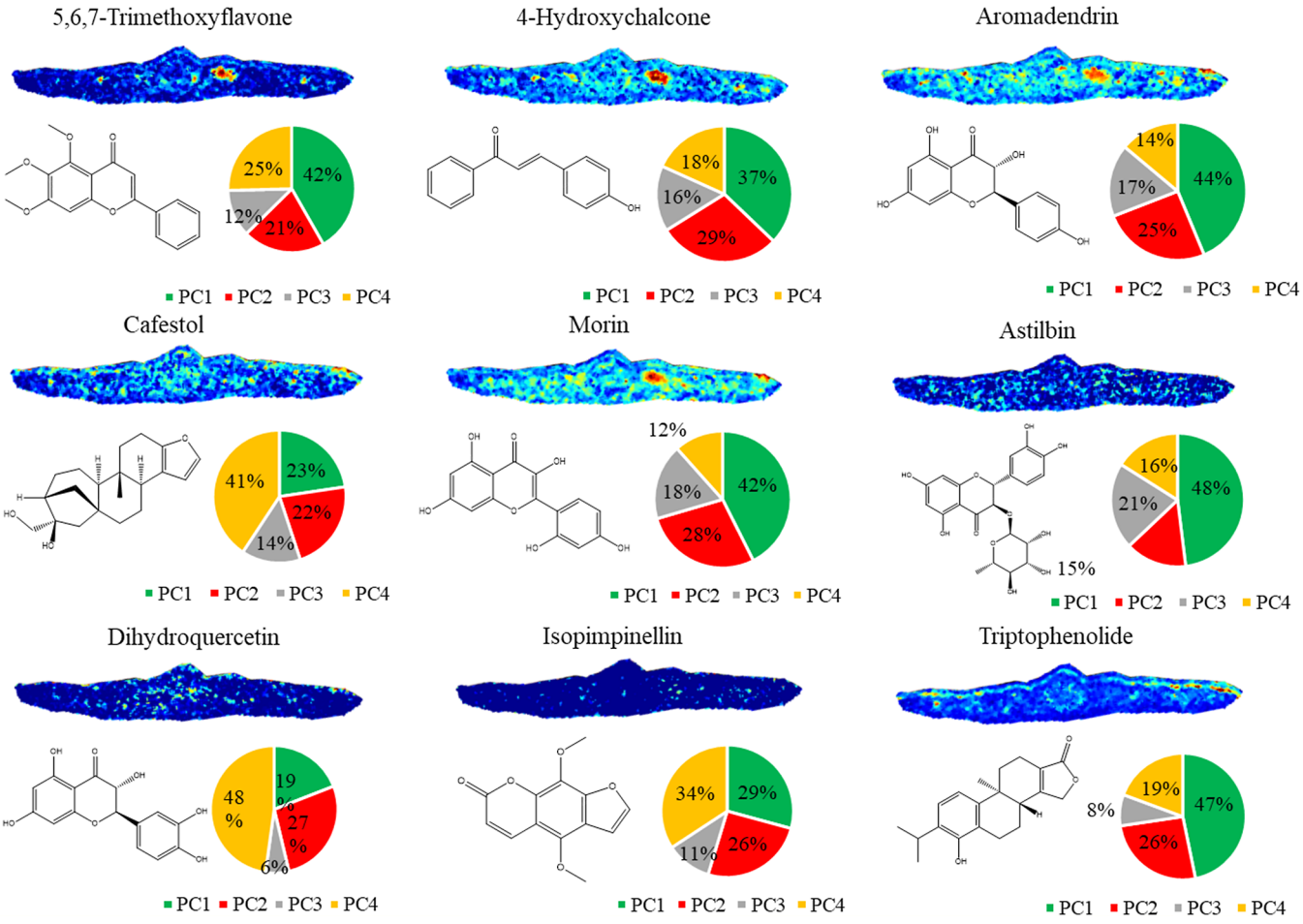

Figure 6. Imaging of relatively uniformly distributed metabolites. Relatively uniformly distributed metabolites were determined by MALDI-IMS analysis. Color scale ranges from 0 to 100%. Blue indicated low accumulation level and red indicated high accumulation level. Proportion of various metabolites in different PCs was showed by pies.

10−20 μm. The tissue sample was transferred from −80 °C to a precooled slicer at −20 °C for 1 h. After adjustment of the angle and orientation, the tissue sample was sliced according to the instructions. The cut slices were transferred onto a MALDI2 specific conductive glass slide (BRUKER, Luken, Germany) and then vacuum-dried for 30 min. After vacuum packaging, the samples were kept at −80 °C until used.

Matrix Spraying and MS Imaging. Commercialized MALDI-2 special matrix solution purchased from BRUKER OPTICS (BRUKER, Luken, Germany) was evenly sprayed onto the special conductive glass slide containing tissue slices using the TM-Sprayer M3 instrument (HTX, Boston, USA). The MALDI-2 special matrix solution: 5 mg/mL of α-cyano-4-hydroxy-cinnamic acid was dissolved in 70% HPLC grade acetonitrile with 0.1% trifluoroacetic acid. The parameters of the matrix application set in the TM-sprayer (HTX, Boston, USA) were as follows: spray nozzle velocity (1200 mm/min), track spacing (2 mm), flow rate (0.12 mL/min), spray nozzle temperature (72 °C), and nitrogen gas pressure (10 psi).

The conductive glass slide with the substrate was placed onto the target disk of TimsTOF flex MALDI2. Metabolites in the samples were imaged using a timsTOF fleX MALDI 2 (BRUKER, Luken, Germany) equipped with a 10 kHz smart beam 3D laser. MALDI2MSI was operated in positive ion mode in full scan mode for m/z 50−1500. MALDI2MSI was performed at a 50 μm spatial resolution. The frequency of the laser was set to 10,000 Hz, with 62% laser energy and 100 laser shots per 50 μm pixel. All molecules were released by ionization at the target site to produce the raw MS imaging data file.

Analysis Procedures of MS Imaging Data. The raw imaging data was imported into SCiLSLab 2021 software (BRUKER, Luken, Germany) for MS analyses. To obtain the average mass spectrum of the region of interest, several data analyses were performed, including baseline subtraction, peak alignment, smoothing, and data normalization. To provide reliable data for spatial denoising and segmentation of the sample region, the datasets were normalized using the SCiLSLab 2021 software (BRUKER, Luken, Germany) with the "root mean square" method. Each pixel in the spatial metabolic profile is independently detected and generated by the MS imaging system. The imaging pixels of the target area were clustered by using the K-Means analysis function in SCiLS In Lab 2021 software (BRUKER, Luken, Germany).

Regions with similar metabolite accumulation patterns were labeled with the same color. PCA was conducted to analyze the distribution of metabolites on the slices, and several PCs were obtained to represent different imaging modes. Each PC was a linear combination of all of the features.

Metabolite Identification. The collected MS imaging data was peak extracted and calibrated using a Bruker MetaboScape workstation (BRUKER, Luken, Germany). The

https://doi.org/10.1021/acsomega.4c01440
ACS Omega 2024, 9, 18634−18642

results with a molecular mass error < 10 ppm were compared with the theoretical mass in the Bruker Library MS Metabase 3.0 database (BRUKER, Luken, Germany). Furthermore, each MS feature was searched against the Kyoto Encyclopedia of Genes and Genomes database for metabolic pathway analysis.

Statistical Analysis. Area under curve > 0.7 or <0.3 and corrected P value < 0.01 were used to screen significant changed metabolites. The P values were adjusted for multiple testing correction by false discovery rate (FDR; Benjamini–Hochberg). SCiLSLab 2021 software was used for statistical analysis.

■ ASSOCIATED CONTENT

Data Availability Statement

The datasets generated and analyzed in the current study are available at Baidu Netdisk (https://pan.baidu.com/s/1hXL8X9bCF5ZLi4UGKXRlHQ [password: tjhg]).

Supporting Information

The Supporting Information is available free of charge at https://pubs.acs.org/doi/10.1021/acsomega.4c01440.

Detailed information on 3387 metabolites with annotations and ROC analysis (XLSX)

Selection of regions of interest for ROC analysis (PDF)

■ AUTHOR INFORMATION

Corresponding Authors

Chenjia Shen − *College of Life and Environmental Sciences, Hangzhou Normal University, Hangzhou 311121, China; Zhejiang Provincial Key Laboratory for Genetic Improvement and Quality Control of Medicinal Plants, Hangzhou Normal University, Hangzhou 311121, China;* orcid.org/0000-0002-8575-0593; Phone: +86-571-28865198; Email: shencj@hznu.edu.cn; Fax: +86-571-28865198

Yan Jiang − *College of Pharmacy, Hangzhou Normal University, Hangzhou 311121, China*; Phone: +86-571-28865198; Email: 840423924@qq.com; Fax: +86-571-28865198

Authors

Xiaori Zhan − *College of Life and Environmental Sciences, Hangzhou Normal University, Hangzhou 311121, China; Zhejiang Provincial Key Laboratory for Genetic Improvement and Quality Control of Medicinal Plants, Hangzhou Normal University, Hangzhou 311121, China*

Yue Zang − *College of Life and Environmental Sciences, Hangzhou Normal University, Hangzhou 311121, China; Zhejiang Provincial Key Laboratory for Genetic Improvement and Quality Control of Medicinal Plants, Hangzhou Normal University, Hangzhou 311121, China*

Ruoyun Ma − *College of Life and Environmental Sciences, Hangzhou Normal University, Hangzhou 311121, China; Zhejiang Provincial Key Laboratory for Genetic Improvement and Quality Control of Medicinal Plants, Hangzhou Normal University, Hangzhou 311121, China*

Wanting Lin − *College of Life and Environmental Sciences, Hangzhou Normal University, Hangzhou 311121, China; Zhejiang Provincial Key Laboratory for Genetic Improvement and Quality Control of Medicinal Plants, Hangzhou Normal University, Hangzhou 311121, China*

Xiao-lin Li − *State Key Laboratory Breeding Base of Dao-di Herbs, National Resource Center for Chinese Materia Medica, China Academy of Chinese Medical Sciences, Beijing 100700, China*

Yanyan Pei − *College of Pharmacy, Hangzhou Normal University, Hangzhou 311121, China*

Complete contact information is available at: https://pubs.acs.org/10.1021/acsomega.4c01440

Author Contributions

X.Z. and C.S. conceptualized the initial study; Y.Z., R.M., and W.L. were involved in the experimental layout; Y.Z., X.-l.L., and W.L. performed the lab experiments, Y.J. and C.S. drafted the initial article; all authors discussed the results, reviewed the article, and approved the final article.

Funding

This work was funded by the National Natural Science Foundation of China (32271905) and the Zhejiang Provincial Natural Science Foundation of China under grant no. LY23C160001. There is no role of the funding body in the design of the study, the collection, analysis, and interpretation of data, and in writing the manuscript.

Notes

The authors declare no competing financial interest.

This project uses plant materials and does not utilize transgenic technology. We complied with all relevant institutional, national, and international guidelines, and the appropriate permissions were obtained from the Mount Changbai National Nature Reserve. The authorities responsible for the Taxus resources are the Mount Changbai National Nature Reserve, who provided permission to collect the samples of *T. cuspidata* for our scientific research.

■ ACKNOWLEDGMENTS

We are grateful to Shanghai Applied Protein Technology Co., Ltd. (Shanghai, China) for the metabolomic analysis.

■ ABBREVIATIONS

MALDI-2, matrix-assisted laser desorption/ionization-2; MS, mass spectrometry; PCA, principal component analysis; KEGG, Kyoto encyclopedia of genes and genomes; PC, principal component

■ REFERENCES

(1) Yu, C.; Huang, J.; Wu, Q.; Zhang, C.; Li, X. L.; Xu, X.; Feng, S.; Zhan, X.; Chen, Z.; Wang, H.; et al. Role of female-predominant MYB39-bHLH13 complex in sexually dimorphic accumulation of taxol in Taxus media. *Hortic. Res.* **2022**, *9*, uhac062.

(2) Sanchez-Munoz, R.; Bonfill, M.; Cusido, R. M.; Palazon, J.; Moyano, E. Advances in the regulation of in vitro paclitaxel production: methylation of a Y-patch promoter region alters BAPT gene expression in Taxus cell cultures. *Plant Cell Physiol.* **2018**, *59* (11), 2255−2267.

(3) Feng, S.; Hou, K.; Zhang, H.; Chen, C.; Huang, J.; Wu, Q.; Zhang, Z.; Gao, Y.; Wu, X.; Wang, H.; et al. Investigation of the role of TmMYB16/123 and their targets (TmMTP1/11) in the tolerance of Taxus media to cadmium. *Tree Physiol.* **2023**, *43* (6), 1009−1022.

(4) Cai, Q.; Song, Q.; Jiang, K.; Lin, Y.; Zhang, Y.; Zhang, J.; Lin, S.; Huang, L.; Xue, Q.; Huang, Z.; et al. Quality evaluation of compounds in leaves of six Taxus species based on UPLC-MS/MS and chemometrics. *Front. Chem.* **2023**, *11*, 1193188.

(5) Gai, Q. Y.; Jiao, J.; Wang, X.; Liu, J.; Fu, Y. J.; Lu, Y.; Wang, Z. Y.; Xu, X. J. Simultaneous determination of taxoids and flavonoids in twigs and leaves of three Taxus species by UHPLC-MS/MS. *J. Pharm. Biomed. Anal.* **2020**, *189*, 113456.

(6) Yu, C.; Luo, X.; Zhang, C.; Xu, X.; Huang, J.; Chen, Y.; Feng, S.; Zhan, X.; Zhang, L.; Yuan, H.; et al. Tissue-specific study across the stem of Taxus media identifies a phloem-specific TmMYB3 involved in the transcriptional regulation of paclitaxel biosynthesis. *Plant J. Cell Mol. Biol.* **2020**, *103* (1), 95−110.
(7) Li, M.; Geng, W.; Wang, Z.; Wang, Q.; Pang, L.; Wang, B.; Wang, P.; Qu, F.; Zhang, X. Analysis of the utilization value of different tissues of Taxus×Media based on metabolomics and antioxidant activity. *BMC Plant Biol.* **2023**, *23* (1), 285.
(8) Meimei, C.; Fengzhen, W.; Huangwei, L.; Candong, L.; Zhaoyang, Y. Discovery of Taxus chinensis fruit wine as potentially functional food against Alzheimer's disease by UHPLC-QE-MS/MS, network pharmacology and molecular docking. *J. Food Biochem.* **2022**, *46* (12), No. e14502.
(9) Tabaszewska, M.; Antoniewska, A.; Rutkowska, J.; Skoczylas, L.; Slupski, J.; Skoczen-Slupska, R. Bioactive Components, Volatile Profile and In Vitro Antioxidative Properties of Taxus baccata L. Red Arils. *Molecules* **2021**, *26* (15), 4474.
(10) Wei, Q.; Li, Q. Z.; Wang, R. L. Flavonoid Components, Distribution, and Biological Activities in Taxus: A review. *Molecules* **2023**, *28* (4), 1713.
(11) Elansary, H. O.; Szopa, A.; Kubica, P.; A Al-Mana, F.; Mahmoud, E. A.; Zin El-Abedin, T. K. A.; A Mattar, M.; Ekiert, H. Phenolic Compounds of Catalpa speciosa, Taxus cuspidate, and Magnolia acuminata have Antioxidant and Anticancer Activity. *Molecules* **2019**, *24* (3), 412.
(12) Hafezi, K.; Hemmati, A. A.; Abbaszadeh, H.; Valizadeh, A.; Makvandi, M. Anticancer activity and molecular mechanisms of α-conidendrin, a polyphenolic compound present in Taxus yunnanensis, on human breast cancer cell lines. *Phytother. Res.* **2020**, *34* (6), 1397−1408.
(13) Zhan, X.; Qiu, T.; Zhang, H.; Hou, K.; Liang, X.; Chen, C.; Wang, Z.; Wu, Q.; Wang, X.; Li, X. L.; et al. Mass spectrometry imaging and single-cell transcriptional profiling reveal the tissue-specific regulation of bioactive ingredient biosynthesis in Taxus leaves. *Plant Commun.* **2023**, *4*, 100630.
(14) Yousaf, A.; Waseem, M.; Javed, A.; Baig, S.; Ismail, B.; Baig, A.; Shahzadi, I.; Nawazish, S.; Zaman, I. Augmented anticancer effect and antibacterial activity of silver nanoparticles synthesized by using Taxus wallichiana leaf extract. *PeerJ* **2022**, *10*, No. e14391.
(15) Kalve, S.; De Vos, D.; Beemster, G. T. Leaf development: a cellular perspective. *Front. Plant Sci.* **2014**, *5*, 362.
(16) Hieta, J. P.; Sipari, N.; Raikkonen, H.; Keinanen, M.; Kostiainen, R. Mass Spectrometry Imaging of Arabidopsis thaliana Leaves at the Single-Cell Level by Infrared Laser Ablation Atmospheric Pressure Photoionization (LAAPPI). *J. Am. Soc. Mass Spectrom.* **2021**, *32* (12), 2895−2903.
(17) Tang, X.; Zhao, M.; Chen, Z.; Huang, J.; Chen, Y.; Wang, F.; Wan, K. Visualizing the spatial distribution of metabolites in Clausena lansium (Lour.) skeels using matrix-assisted laser desorption/ionization mass spectrometry imaging. *Phytochemistry* **2021**, *192*, 112930.
(18) Etalo, D. W.; Díez-Simón, C.; de Vos, R. C. H.; Hall, R. D. Laser Ablation Electrospray Ionization-Mass Spectrometry Imaging (LAESI-MS) for Spatially Resolved Plant Metabolomics. *Methods Mol. Biol.* **2018**, *1778*, 253−267.
(19) Maia, M.; McCann, A.; Malherbe, C.; Far, J.; Cunha, J.; Eiras-Dias, J.; Cordeiro, C.; Eppe, G.; Quinton, L.; Figueiredo, A.; et al. Grapevine leaf MALDI-MS imaging reveals the localisation of a putatively identified sucrose metabolite associated to Plasmopara viticola development. *Front. Plant Sci.* **2022**, *13*, 1012636.
(20) Ozdemir, A.; Lin, J.-L.; Gulfen, M.; Chen, C.-H. Advancing mass spectrometry-based chemical imaging: A noncontact continuous flow surface probe in mass spectrometry for enhanced signal detection and spatial resolution. *Talanta* **2024**, *273*, 125858.
(21) Fan, W.; Yang, Y.; Li, L.; Fan, L.; Wang, Z.; Yang, L. Mass spectrometry-based profiling and imaging strategy, a fit-for-purpose tool for unveiling the transformations of ginsenosides in Panax notoginseng during processing. *Phytomedicine* **2022**, *103*, 154223.
(22) Ho, Y. N.; Shu, L. J.; Yang, Y. L. Imaging mass spectrometry for metabolites: technical progress, multimodal imaging, and biological interactions. *Wiley Interdiscip. Rev.: Syst. Biol. Med.* **2017**, *9* (5), No. e1387.
(23) Konishi, T. Principal component analysis for designed experiments. *BMC Bioinformatics* **2015**, *16* (S18), S7.
(24) Kan, S. L.; Shen, T. T.; Gong, P.; Ran, J. H.; Wang, X. Q. The complete mitochondrial genome of Taxus cuspidata (Taxaceae): eight protein-coding genes have transferred to the nuclear genome. *BMC Evol. Biol.* **2020**, *20* (1), 10.
(25) Zhang, S.; Lu, X.; Zheng, T.; Guo, X.; Chen, Q.; Tang, Z. Investigation of bioactivities of Taxus chinensis, Taxus cuspidata, and Taxus × media by gas chromatography-mass spectrometry. *Open Life Sci.* **2021**, *16* (1), 287−296.
(26) Zhang, M.; Lu, X.; Zhang, J.; Zhang, S.; Dong, M.; Huo, C.; Shi, Q.; Gu, Y.; Cong, B. Taxanes from the leaves of Taxus cuspidata. *Chem. Nat. Compd.* **2010**, *46* (1), 53−58.
(27) Zhan, X.; Zhang, H.; Liang, X.; Kailin, H.; Lin, W.; Ma, R.; Qiu, T.; Chen, C.; Wang, Z.; Wu, Q.; et al. Single-cell ATAC sequencing illuminates the cis-regulatory differentiation of taxol biosynthesis between leaf mesophyll and leaf epidermal cells in Taxus mairei. *Ind. Crops Prod.* **2023**, *205*, 117411.
(28) Casapullo, A.; Cutignano, A.; Bruno, I.; Bifulco, G.; Debitus, C.; Gomez-Paloma, L.; Riccio, R. Makaluvamine P, a New Cytotoxic Pyrroloiminoquinone from Zyzzya cf. fuliginosa. *J. Nat. Prod.* **2001**, *64* (10), 1354−1356.
(29) Samie, A.; Sedaghat, R.; Baluchnejadmojarad, T.; Roghani, M. Hesperetin, a citrus flavonoid, attenuates testicular damage in diabetic rats via inhibition of oxidative stress, inflammation, and apoptosis. *Life Sci.* **2018**, *210*, 132−139.
(30) He, W.; Chen, W.; Zhou, Y.; Tian, Y.; Liao, F. Xanthotoxol exerts neuroprotective effects via suppression of the inflammatory response in a rat model of focal cerebral ischemia. *Cell. Mol. Neurobiol.* **2013**, *33* (5), 715−722.
(31) Pieroni, A.; Pachaly, P. Isolation and structure elucidation of ligustroflavone, a new apigenin triglycoside from the leaves of Ligustrum vulgare L. *Pharmazie* **2000**, *55* (1), 78−80.
(32) Akram, W.; Yasin, N. A.; Shah, A. A.; Khan, W. U.; Li, G.; Ahmad, A.; Ahmed, S.; Hussaan, M.; Rizwan, M.; Ali, S. Exogenous application of liquiritin alleviated salt stress and improved growth of Chinese kale plants. *Sci. Hortic.* **2022**, *294*, 110762.
(33) Tuan Anh, H. L.; Trang, D. T.; Tuan, D. T.; Duc, T. M.; Phuong Anh, T. T.; Hai Yen, D. T.; Nhiem, N. X.; Minh, C. V.; Tai, B. H.; Kiem, P. V. Dipeptide and phenolic compounds from the leaves of Cudrania tricuspidata Carr. Bur and their cytotoxic activity. *Vietnam J. Chem.* **2015**, *53* (5), 580.
(34) Wang, L.; Tanveer, M.; Wang, H.; Arnao, M. B. Melatonin as a key regulator in seed germination under abiotic stress. *J. Pineal Res.* **2024**, *76* (1), No. e12937.
(35) Li, N.; Liu, T.; Zhu, S.; Yang, Y.; Wang, Z.; Zhao, Z.; Liu, T.; Wang, X.; Qin, W.; Yan, Y.; et al. Corylin from Psoralea fructus (Psoralea corylifolia L.) protects against UV-induced skin aging by activating Nrf2 defense mechanisms. *Phytother. Res.* **2022**, *36* (8), 3276−3294.
(36) Zhang, L.; Liao, C. C.; Huang, H. C.; Shen, Y. C.; Yang, L. M.; Kuo, Y. H. Antioxidant phenylpropanoid glycosides from Smilax bracteata. *Phytochemistry* **2008**, *69* (6), 1398−1404.
(37) Dymarska, M.; Grzeszczuk, J.; Urbaniak, M.; Janeczko, T.; Pląskowska, E.; Stępień, Ł.; Kostrzewa-Susłow, E. Glycosylation of 6-methylflavone by the strain Isaria fumosorosea KCH J2. *PLoS One* **2017**, *12* (10), No. e0184885.
(38) Korte, A. R.; Yandeau-Nelson, M. D.; Nikolau, B. J.; Lee, Y. J. Subcellular-level resolution MALDI-MS imaging of maize leaf metabolites by MALDI-linear ion trap-Orbitrap mass spectrometer. *Anal. Bioanal. Chem.* **2015**, *407* (8), 2301−2309.
(39) Safa, N.; Trobec, T.; Holland, D. C.; Slazak, B.; Jacobsson, E.; Hawkes, J. A.; Frangež, R.; Sepčić, K.; Göransson, U.; Moodie, L. W. K.; et al. Spatial Distribution and Stability of Cholinesterase Inhibitory

https://doi.org/10.1021/acsomega.4c01440
ACS Omega 2024, 9, 18634−18642

Protoberberine Alkaloids from Papaver setiferum. *J. Nat. Prod.* **2022**, *85* (1), 215−224.
(40) Saini, N.; Grewal, A. S.; Lather, V.; Gahlawat, S. K. Natural alkaloids targeting EGFR in non-small cell lung cancer: Molecular docking and ADMET predictions. *Chem.-Biol. Interact.* **2022**, *358*, 109901.
(41) Oetari, R. A.; Hasriyani, H.; Prayitno, A.; Sahidin, S. Gartanin Compounds from Extract Ethanol Pericarp Mangosteen (Garcinia mangostana Linn.). *Open Access Maced. J. Med. Sci.* **2019**, *7* (22), 3891−3895.
(42) Pham, V.; Rendon, R.; Le, V. X.; Tippin, M.; Fu, D. J.; Le, T. H.; Miller, M.; Agredano, E.; Cedano, J.; Zi, X. Gartanin is a novel NEDDylation inhibitor for induction of Skp2 degradation, FBXW2 expression, and autophagy. *Mol. Carcinog.* **2020**, *59* (2), 193−201.
(43) Zhuan, Q.; Li, J.; Du, X.; Zhang, L.; Meng, L.; Luo, Y.; Zhou, D.; Liu, H.; Wan, P.; Hou, Y.; et al. Antioxidant procyanidin B2 protects oocytes against cryoinjuries via mitochondria regulated cortical tension. *J. Anim. Sci. Biotechnol.* **2022**, *13* (1), 95.
(44) Kim, D. H.; Yun, B. H.; Choi, E. W.; Oh, S. M.; Alam, M. M.; Lee, K. T.; Lee, Y. S. Synthesis and Cytotoxic Effects of Sulfonamide-Substituted 5,6,7-Trimethoxyflavones on Human Cancer Cell Lines. *Bulletin of the Korean Chemical Society* **2013**, *34* (8), 2507−2510.
(45) Marwa, E.; Abeer, M.; Mona, H. Cytotoxicity and chromatographic analysis of Dioon spinulosum, family Zamiaceae. *J. Appl. Pharm. Sci.* **2020**, *10* (12), 075−082.
(46) Grigolon, G.; Nowak, K.; Poigny, S.; Hubert, J.; Kotland, A.; Waldschütz, L.; Wandrey, F. From Coffee Waste to Active Ingredient for Cosmetic Applications. *Int. J. Mol. Sci.* **2023**, *24* (10), 8516.
(47) Sunil, C.; Xu, B. An insight into the health-promoting effects of taxifolin (dihydroquercetin). *Phytochemistry* **2019**, *166*, 112066.
(48) de Jesús Acosta-Cota, S.; Aguilar-Medina, E. M.; Ramos-Payán, R.; Rendón Maldonado, J. G.; Romero-Quintana, J. G.; Montes-Avila, J.; Sarmiento-Sánchez, J. I.; Plazas-Guerrero, C. G.; Vergara-Jiménez, M. J.; Sánchez-López, A.; et al. Therapeutic effect of treatment with metformin and/or 4-hydroxychalcone in male Wistar rats with nonalcoholic fatty liver disease. *Eur. J. Pharmacol.* **2019**, *863*, 172699.
(49) Sinha, K.; Sadhukhan, P.; Saha, S.; Pal, P. B.; Sil, P. C. Morin protects gastric mucosa from nonsteroidal anti-inflammatory drug, indomethacin induced inflammatory damage and apoptosis by modulating NF-kappa B pathway. *Biochim. Biophys. Acta, Gen. Subj.* **2015**, *1850* (4), 769−783.
(50) Wang, D.; Li, S.; Chen, J.; Liu, L.; Zhu, X. The Effects of Astilbin on Cognitive Impairments in a Transgenic Mouse Model of Alzheimer's Disease. *Cell. Mol. Neurobiol.* **2017**, *37* (4), 695−706.
(51) Patterson, N. H.; Tuck, M.; Van de Plas, R.; Caprioli, R. M. Advanced Registration and Analysis of MALDI Imaging Mass Spectrometry Measurements through Autofluorescence Microscopy. *Anal. Chem.* **2018**, *90* (21), 12395−12403.
(52) Chen, J.; Zhong, K.; Jing, Y.; Liu, S.; Qin, S.; Peng, F.; Li, D.; Peng, C. Procyanidin B2: A promising multi-functional food-derived pigment for human diseases. *Food Chem.* **2023**, *420*, 136101.

https://doi.org/10.1021/acsomega.4c01440
ACS Omega 2024, 9, 18634−18642